Predictable topological sensitivity of Turing patterns on graphs

Marc-Thorsten Hütt, Dieter Armbruster, Annick Lesne

Predictable Topological Sensitivity of Turing Patterns on Graphs

Marc-Thorsten Hütt*
Department of Life Sciences and Chemistry, Jacobs University, D-28759 Bremen, Germany

Dieter Armbruster†
School of Mathematical and Statistical Sciences, Arizona State University, Tempe, AZ 85281

Annick Lesne‡
Institut de Génétique Moléculaire de Montpellier, University of Montpellier, CNRS, F-34293, Montpellier, France and Sorbonne Université, CNRS, Laboratoire de Physique Théorique de la Matière Condensée, LPTMC, F-75252, Paris, France

(Dated: December 22, 2021)

Reaction-diffusion systems implemented as dynamical processes on networks have recently renewed the interest in their self-organized collective patterns known as Turing patterns. We investigate the influence of network topology on the emerging patterns and their diversity, defined as the variety of stationary states observed with random initial conditions and the same dynamics. We show that a seemingly minor change, the removal or rewiring of a single link, can prompt dramatic changes in pattern diversity. The determinants of such critical occurrences are explored through an extensive and systematic set of numerical experiments. We identify situations where the topological sensitivity of the attractor landscape can be predicted without a full simulation of the dynamical equations, from the spectrum of the graph Laplacian and the linearized dynamics. Unexpectedly, the main determinant appears to be the degeneracy of the eigenvalues or the growth rate and not the number of unstable modes.

INTRODUCTION

Turing's idea [1] of pattern formation through the interaction of chemical species via nonlinear reaction-diffusion equations had an enormous impact on the biology of morphogenesis [2, 3]. It stood as an emblematic example of a dissipative structure in physics and chemistry [4–6] and offered a mathematical laboratory for the investigation of spatially extended instabilities [7]. It continues to serve as a prototypical example in studies of pattern formation on networks [8].

Indeed [9], in many interesting cases, diffusion acts along links in a network rather than in a continuous space. Mathematically, this implies swapping the Laplace operator for the graph Laplacian L in the diffusion terms of the evolution equations (see *Methods*). Defining vectors $\mathbf{u} = (u_1...u_N)$ and $\mathbf{v} = (v_1...v_N)$ for the activator and inhibitor species, the generic Turing reaction-diffusion model on a network of N nodes is thus written

$$\frac{du_i}{dt} = f(u_i, v_i) + \varepsilon(L\mathbf{u})_i \tag{1}$$

$$\frac{dv_i}{dt} = g(u_i, v_i) + \sigma\varepsilon(L\mathbf{v})_i \quad i = 1..N \tag{2}$$

where ε is the diffusion coefficient of the activator and $\sigma\varepsilon$ that of the inhibitor. We assume that the system has a uniform equilibrium solution $(\bar{u}, \bar{v})$. A pattern will be defined as a non-uniform stationary state, reached after some transients.

Turing understood pattern formation as linear instability of the uniform equilibrium solution i.e. when a parameter crosses an instability threshold an eigenvector of the Laplacian operator exhibits exponential growth which eventually saturates due to nonlinear interactions. In [8] the authors have shown that this mechanism still applies for reaction-diffusion dynamics on networks, where the eigenvectors are now those of the graph Laplacian L.

Since the beginning of the detailed study of complex networks within statistical physics in the late 1990s and early 2000s [10–12], a clear roadmap has emerged: from a topological characterization to the study of dynamical processes on network and, in this way, the search for universal relationships between network structure and network function. These investigations have revolutionized our understanding of complex systems [13–16] and have established themselves as a novel branch of interdisciplinary research.

Among the results in the statistical physics of complex networks the most striking ones are concerned with the emergence of self-organized, collective patterns in dynamics on graphs – with Turing patterns [8] as a prominent example, but also synchronization patterns [17] (see also [18] for a study of resonance patterns in oscillatory networks), growth patterns and clusters [19, 20], waves in networks [21, 22] and many more.

Theoretical studies reveal, how such patterns are enhanced by certain architectural features of the network

* m.huett@jacobs-university.de
† dieter@asu.edu
‡ annick.lesne@sorbonne-universite.fr

[22–24] and transdisciplinary investigations help understand the implications of such patterns for network-like infrastructures [25–31].

Starting from [8], several subsequent studies focused on the impact of network features on Turing pattern formation: In [32] the authors discussed how oriented networks explain subcritical patterns while [33] studied the impact of degree fluctuations in the network. Extensions to pattern formation for FitzHugh-Nagumo dynamics on networks [34], to predator-prey models [35] and to epidemic growth [36] have been presented.

Our study is motivated by an observation for the Gierer-Meinhardt pattern formation model (see *Methods*) on the macaque cortical area network. In this network, nodes are anatomically defined cortical areas of the macaque brain and links represent experimentally verified connections among these areas (we only use connections reported as 'strong' in [37]). Simulating Turing patterns on this network architecture we find that for a fixed set of dynamical parameters and a given graph, but random initial conditions, a large number of different patterns emerges. For other parameter values or different graphs, the dynamics converge to a single pattern. Moreover, one can change the pattern forming process from the former to the latter by small changes in the graph topology. Figure 1 summarizes this observation.

We study quantitatively how small changes in the graph topology can create such drastic changes in the attractor landscape. Numerical investigations were performed for a minimal network model and for random regular graphs. We identify basic spectral determinants of pattern diversity. Mainly, highly diverse pattern formation is observed in degenerate situations, created by almost symmetrical network structures or by nearly identical growth rates of neighboring eigenvectors of the graph Laplacian. We propose a general scheme for predicting the topological sensitivity of Turing pattern diversity, based on the movement on the dispersion curve of Laplacian eigenvalues under network perturbations.

METHODS

Network models

For the *macaque cortical area network* (Fig. 1) each node represents a cortical area built from the publicly available database Core-Nets (core-nets.org; see [38, 39]) following a scheme described in [37]. The Turing patterns obtained on this graph are compared to those obtained after removal of a link between the primary somatosensory cortex (area 2) and the ventral proisocortical area ProM (highlighted in red in Fig. 1A). Note that we use this network only as an illustrative example of the phenomenon of topological sensitivity of Turing patterns. A detailed analysis of pattern formation on this network architecture would require a more careful variation of kinetic parameters, as well as a stronger emphasis on the relevance of such results for neuroscience.

The *ring graph* has nearest neighbor connections and 111 nodes. We attach one end of a shortcut at node $i_0 = 1$ and the other end to nodes $i_s = 2...N$ successively. *Random regular graphs* with degree $k = 4$ are generated for 30 nodes in Fig. 4. Suppl. Fig. S6 shows a random (*Erdős-Rényi* network with 30 nodes and 100 links. The graph Laplacian is defined as $L = A - D$ where A is the $N \times N$ adjacency matrix A. D is the diagonal matrix whose entries are the degree k_i of node i. Since our networks are undirected, L is a symmetric matrix. L always has a zero eigenvalue and is negative-semidefinite (that is $\Lambda_i \leq 0$) [40]. Eigenvalues are labelled in decreasing order $\Lambda_N \leq \Lambda_1 \leq \Lambda_0 = 0$. This definition is consistent with numerical discretization of the Laplace operator, describing diffusion in a continuum but not with standard graph theory where the opposite sign convention is generally adopted ($L = D - A$).

Pattern formation

The Gierer-Meinhardt model [2] is a generic Turing model for an activator species u and a inhibitor species v

$$\begin{array}{rcl} \frac{\partial u}{\partial t} & = & a - bu + \frac{u^2}{v} + \varepsilon L u \\ \frac{\partial v}{\partial t} & = & u^2 - v + \sigma\varepsilon L v. \end{array} \tag{3}$$

The reaction part of the dynamics involves two positive parameters a and b which determine the homogeneous steady state $(\bar{u}, \bar{v}) = ((a+1)/b, (a+1)^2/b^2$. The parameter ϵ is the diffusion coefficient of the activator and $\sigma\epsilon$ is the diffusion coefficient of the inhibitor.

The dispersion relation $\lambda(\Lambda)$ describes the functional dependence of the growth rate λ on the eigenvalues Λ of the graph Laplacian. We linearize eq. 3 around the homogeneous steady state and write the solution as a linear combination of the eigenvectors of the graph Laplacian. The growth rate for the Laplacian eigenvector V_Λ associated with the eigenvalue Λ is [8]

$$\begin{aligned} \lambda(\Lambda) = (1/2)[f_u + g_v + (1+\sigma)\varepsilon\Lambda + \\ \sqrt{4 f_v g_u + (f_u - g_v + (1-\sigma)\varepsilon\Lambda)^2} \end{aligned} \tag{4}$$

where $f_u = (\partial f/\partial u)(\bar{u}, \bar{v})$ is the partial derivative of $f(u, v)$ at the equilibrium point $(\bar{u}, \bar{v})$. The expression for the continuum where the eigenmodes are sinusoids with wave-vector q is recovered by replacing Λ with $-q^2$.

We consider a steady state bifurcation and assume that $\lambda(\Lambda)$ is real, and use σ as a bifurcation parameter. Thus a bifurcation occurs when the dispersion relation moves from negative to positive values, indicating a transition from damped modes to exponentially growing modes. For the Gierer-Meinhardt system eq. 3, this occurs for

$$\sigma_c = \frac{a+1}{b(a-1)^2}(a + 3 + 2\sqrt{2}\sqrt{a+1}). \tag{5}$$

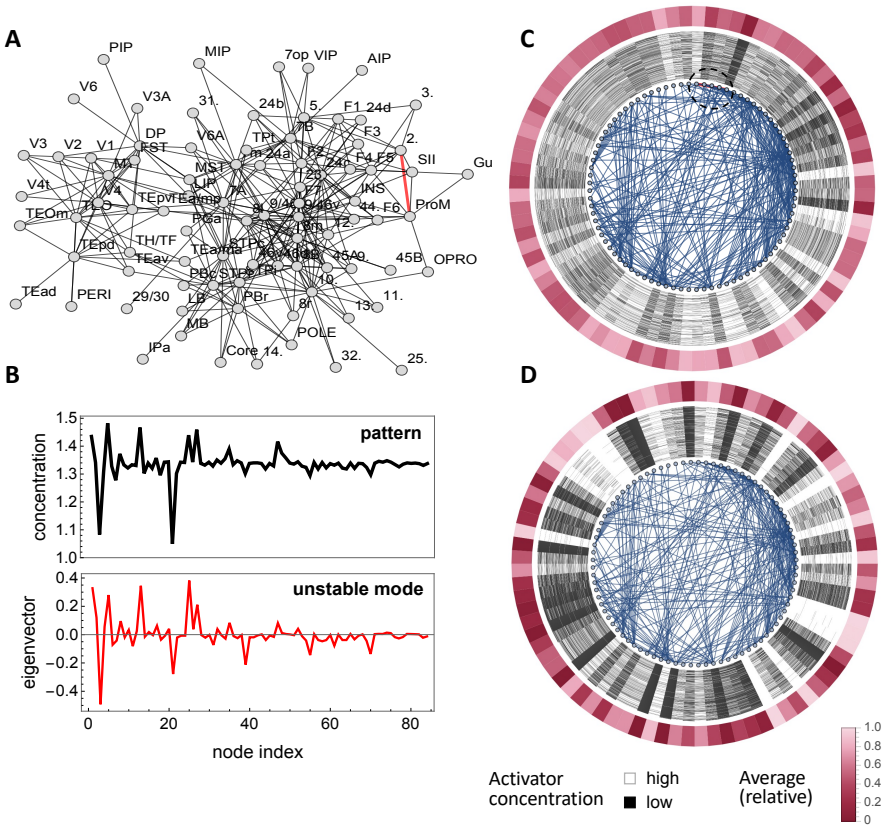

FIG. 1. Topological sensitivity of Turing pattern diversity on the macaque cortical area network. (A) Representation of the macaque cortical area network (see *Methods*). (B) Example of a pattern arising for the Gierer-Meinhardt dynamical model from the sixth eigenvector of the Laplacian matrix of the graph, shown underneath. (C) We arrange the nodes in an arbitrary but fixed way on a circle. The links between the nodes are shown in blue in the center. Each concentric ring represents a binarized Turing pattern originating from a randomly chosen initial condition, in total 500 runs (see *Methods*). The surrounding purple ring shows their average. Panel (D) shows the same pattern wheel representation after removal of a single link (highlighted in red in (A) and (C) [upper left quadrant; see the dashed ellipse]).

The dispersion curve is the plot of the growth rate λ as a function of $\ln(-\Lambda)$ (recall that Laplacian eigenvalues Λ are all negative), as displayed e.g. in Fig. 3. The structure of the network is reflected in the discrete sampling of the horizontal axis by the Laplacian eigenvalues.

Numerical simulations

For a given network and a given set of dynamical parameters ε, σ, a and b a numerical experiment entails 500 runs in *Mathematica* using randomly chosen initial conditions. Since transients appear to decay in less than 500 time steps, the duration of a run was typically 2,000 time steps.

The following parameter selection scheme, which we call growth-rate degeneracy (GRD), was used in the simulation: Parameters are chosen such that two successive eigenvectors have approximately the same positive growth rate. This is achieved by selecting parameters in such a way that the maximum of the dispersion relation at σ_c is exactly midway between the two corresponding eigenvalues of the graph Laplacian. To create a positive growth rate, σ is then increased slightly by an amount $\Delta\sigma = 0.02$ beyond the instability threshold (see Fig. 4).

Pattern evaluation

The pattern wheel representation of multiple simulations of Turing patterns allows for a visual assessment of pattern diversity for the same graph and the same kinetic parameters. Each pattern, characterized through the asymptotic value of the dynamical variable u_i for each node i is binarized using the average over all nodes as a threshold, retaining only the information whether the activator concentration is high or low. The

pattern with the highest correlation to an unstable mode serves as the reference pattern. Each simulated pattern is multiplied by -1, if this increases the visual agreement to the reference pattern (accounting for the fact that a reflected pattern is still generated by the same eigenvector). These aligned and binarized patterns are plotted around a circular embedding of the graph under consideration. Averages over these binarized patterns for each node are then displayed as an outside ring (outer purple ring in the figures).

A *pattern similarity index* is developed to quantitatively assess the diversity of patterns: Let

$$u^{(k)} = \{u_i^{(k)}(t \to \infty)\}_{i=1,\ldots,N}$$

denote the pattern observed in the kth simulation run of a network of N nodes, with $u_i^{(k)}(t \to \infty)$ the asymptotic value of the dynamical variable at node i for run k. We then construct a pattern similarity graph, in which a node is a pattern $u^{(k)}$ and a link between two patterns is generated, if the similarity between these patterns exceeds a threshold θ, leading to the edge set E,

$$E = \{(u^{(k)}, u^{(l)} || \mathrm{corr}(u^{(k)}, u^{(l)})| > \theta\},$$

where $\mathrm{corr}(u^{(k)}, u^{(l)})$ is the Pearson correlation coefficient of two patterns $u^{(k)}$ and $u^{(l)}$,

$$\mathrm{corr}(u^{(k)}, u^{(l)}) = \sum_{i=1}^{N} \frac{(u_i^{(k)} - \bar{u}^{(k)})(u_i^{(l)} - \bar{u}^{(l)})}{\sigma(u^{(k)})\sigma(u^{(l)})}.$$

Here $\bar{u}^{(k)}$ and $\sigma(u^{(k)})$ denote the average and the standard deviation of pattern $u^{(k)}$ over the components i, respectively. Specifically, an edge is drawn between two patterns if the absolute value of their Pearson correlation coefficient exceeds $\theta = 0.9$. The pattern similarity index Π is then defined as the connectivity of this pattern similarity graph, $\Pi = 2|E|/(N(N-1))$.

The correlation analysis in Figure 2C is based on the Pearson correlation coefficient C_i between a pattern and the i-th eigenvector where the index i spans the set of unstable eigenvectors. The maximum correlation strength $\max_i |C_i|$ determines whether a pattern is weakly or strongly correlated with a single eigenvector. Histograms of the correlation strength over 500 patterns generated from random initial conditions reveal two classes: histograms with a marked peak at 1, or broad ones. We interpret a histogram with a broad shape as coming from a pattern that is generated by multiple modes whereas histograms with a peak near one represent patterns generated by a single eigenvector. Similarly, the maximum absolute value of the correlation coefficient between a pattern and a set of unstable modes characterizes how well a given pattern agrees with a single unstable mode, thus offering insight in the *predictability* of this pattern by eigenvectors. Across a whole set of patterns (same parameters, random initial conditions) the set of these maximal absolute values of correlation coefficients – the distribution of pattern predictabilities – is a suitable quantifier of pattern diversity.

The *pattern diversity array* shown in Fig. 4 allows to predict, for a given network, combinations of eigenvectors and links, where pattern diversity is particularly sensitive to the addition or removal of a link. The pattern diversity array – with links of the network enumerated on the horizontal axis and eigenvectors of the network (on which the parameter tuning scheme is centered) enumerated on the vertical axis – offers a color-coded representation of our prediction of changes in pattern diversity for each combination of an eigenvector and a link, for the GRD parameter selection scheme described above. Colors coding is summarized in Fig. 4.

A MINIMAL MODEL: THE RING GRAPH WITH ONE SHORTCUT

We first investigate the topological sensitivity of Turing pattern formation in a minimal network model, composed of a ring graph with one moveable shortcut.

Turing pattern diversity changes under small topological variations are shown in Figure 2 for a ring with a single shortcut. A similar model has been introduced in [41] to study the influence of the topology of the underlying graph on pattern formation by a cellular automaton. The two pattern wheel representations, Figures 2A and 2B, representing different shortcut positions, show very different pattern diversity. As this model is very simple, we can analyze it like a spatially extended system. Symmetric bifurcation theory [42] states that eigenvalues of the ring graph Laplacian are degenerate with multiplicity 2 and the eigenvectors are sinusoids. Adding a single shortcut to the ring breaks the symmetry of the graph and thus the degeneracy of the eigenvalues. Supplementary Figure S1 provides an overview of spectra and eigenvectors for the ring graph and a ring graph with one shortcut.

As a consequence of the shortcut-induced symmetry breaking, one of the degenerate eigenvalues is independent of the shortcut leading to the same sinusoidal pattern as for the ring graph. The other eigenvalue changes.

Figure 2C shows that the other eigenvalue moves, returning periodically to the degenerate situation, as the shortcut is moved around the ring graph.

Since changing the graph does not change the dispersion relation $\lambda(\Lambda)$ (i.e. the expression of the growth rate λ of an eigenmode as a function of the eigenvalue Λ, see Methods), the interval on the dispersion relation that leads to growing patterns is unaffected. Thus, we can set the dynamical parameters in such a way, that some eigenvectors of the Laplacian lead to growing pattern for all shortcut positions while other eigenvectors correspond to eigenvalues moving in and out of this interval, as in-

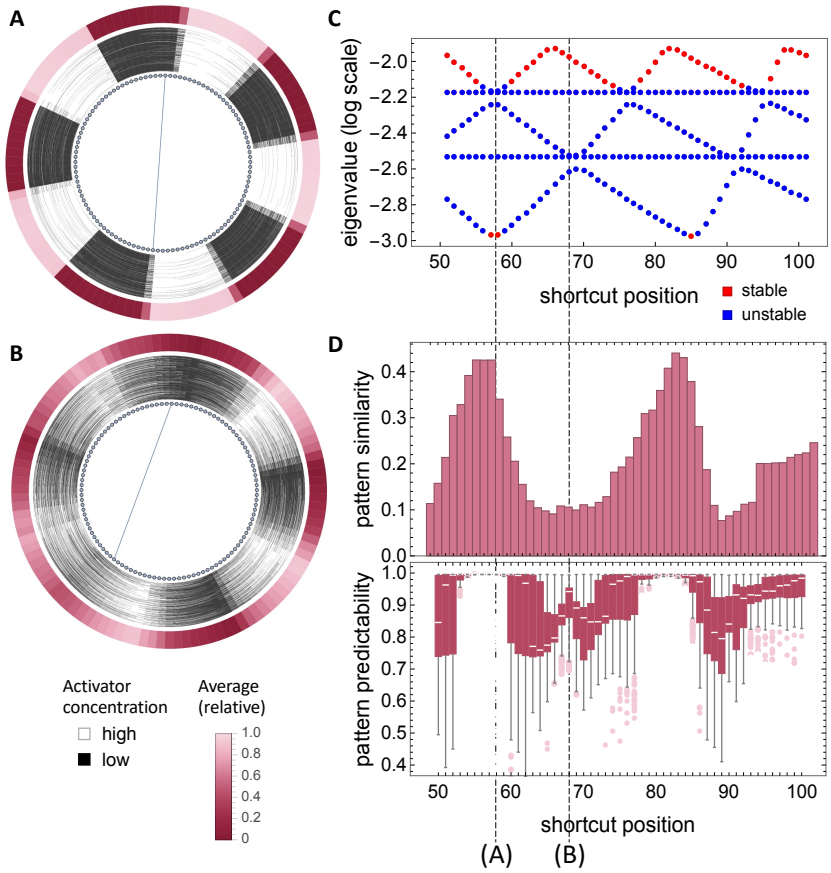

FIG. 2. Topological sensitivity of Turing pattern diversity on the ring graph with one shortcut. (A) Pattern wheel representation for a ring graph of $N = 111$ nodes with a shortcut from node 1 to node 58. A global attraction to a single pattern independent of the initial condition is observed. (B) Same as (A), but for a shortcut from node 1 to node 68; now each observed pattern depends on the specific initial condition. (C) Evolution of eigenvalues for the ring graph with one shortcut as a function of the shortcut position (i.e., the endpoint of the shortcut, the starting point being kept fixed). Note that only eigenvalues which are unstable for some shortcut position are shown. (D) Top panel: Pattern similarity index (see *Methods*) as a function of the shortcut position. Bottom panel: Pattern predictability distributions (see *Methods*), depicting the correlation between patterns and unstable eigenvectors. The two shortcut positions for (A) and (B) are highlighted as dashed lines. The distribution of pattern predictability is shown as a sequence of box plots (white lines in the middle of the red bars indicating the median; size of the bar are the 25% and 75% quantiles; error bars ('whiskers') are the range of values covered with the exception of outliers, which are shown as additional light-red points).

dicated by blue (growing pattern) and red dots (stable homogeneous solution). Supplementary Figure S2 illustrates the movement of eigenvalues as a function of the shortcut position (Fig. 2C) via snapshots of the dispersion relation (see also Supplementary Movie 1). All of these findings can be analytically shown using an extension of the interlacing theorem [43, 44] and linear operator theory for spatially extended systems (see *Appendix A*).

The impact of the changes in the spectrum of the graph Laplacian on pattern diversity is measured in Fig. 2D. The top panel presents the similarity measure of the set of patterns observed for 500 random initial conditions as a function of the shortcut position. An alternative visualization is presented in the bottom panel, summarizing as a box-plot the correlation between the unstable eigenvectors and the patterns obtained by numerically solving the Turing dynamical system starting from randomly chosen initial conditions. Further analysis (see Appendix) shows that the shortcut position in Fig. 2(B) corresponds to almost exactly one wavelength of the pattern (within limits of the discretization due to the finite number of nodes) and hence does not break the rotational symmetry of the ring graph (more detail in Suppl. Figs. S3 and S4). As a result there is a free phase leading to a low pattern similarity and low pattern predictability. For shortcut position (A) the spectrum has a large gap between the central mode on

the dispersion relation (the eigenvalue with the largest growth rate) and the neighboring unstable modes. In fact, although the top three eigenvalues are unstable and very close, since their growth rates are very weak, the central mode is very far from being degenerate and thus dominates the pattern formation (see also Suppl. Fig. S4, panels A and B). As a result, pattern similarity between patterns is high and the resulting pattern is almost deterministically predictable. Note that in this case four eigenvectors of the graph Laplacian are unstable whereas in shortcut position B only three are unstable suggesting that the driver of pattern diversity is not the number of unstable modes but the gap between the dominant mode and the neighboring modes. As a result, topological sensitivity of pattern diversity depends on the changes in the eigenvalue spectrum with eigenvalue degeneracy at maximal growth rate being most susceptible to topological changes. Suppl. Figs. S3 and S4 show additional quantitative details. Specifically, Suppl. Fig. S3 panel D shows high pattern diversity without an eigenvalue degeneracy. Instead the growth rate of two neighboring eigenvectors are very similar. This suggests that there may be a second mechanism involved in the generation and destruction of a high diversity of pattern which we call *growth rate degeneracy*.

PATTERN DIVERSITY ON RANDOM GRAPHS

Next, we explore the topological sensitivity of Turing pattern formation and the role of growth rate degeneracy (GRD) for random regular graphs. In random regular graphs, all nodes have the same degree but are otherwise randomly connected.

Emergence of a Turing pattern on a random regular graph follows the paradigm established for the minimal model: For a single unstable mode of a dispersion relation, starting from random initial conditions the asymptotic pattern agrees well with the unstable eigenvector.

No analytic results can be formulated for random regular graphs. However we developed predictive criteria for pattern diversity and for topological sensitivity based on the spectrum of the Laplacian. They have been validated in a large numerical experiment. Figure 3 shows the experimental setup: We adjust the dynamical parameters such that the growth rate for an eigenvector e_k is the same as for the adjacent eigenvector e_{k+1}. Since the dispersion relation is locally quadratic, this is achieved by putting its maximum exactly in the middle between two neighboring eigenvalues of the Laplacian. We call this the GRDON parameter selection scheme (GRD in the original network). The GRDPN parameter selection scheme generates the reverse changes: we select dynamical parameters such that the maximum of the dispersion relation is between two eigenvalues of the *perturbed* network, i.e. *after* the deletion of a link in the original graph.

The GRDON parameter selection scheme is designed to search for cases, where link removal decreases pattern diversity (as we start from a situation – growth rate degeneracy – predicted to favor pattern diversity). In order to systematically search for situations, where link removal can increase pattern diversity, we need to start from a non-degenerate setup and arrive at an approximate growth rate degeneracy. The purpose of the GRDPN scheme is to systematically search for such situations, as by construction upon link removal we arrive at an approximate growth rate degeneracy.

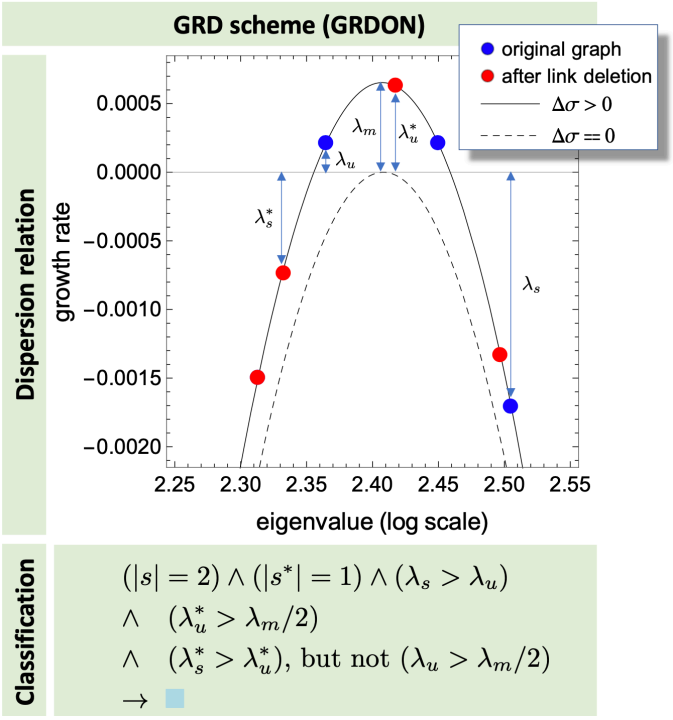

FIG. 3. The dispersion curve for the parameter selection scheme GRDON. The top panel illustrates the quantities involved in the predictability criteria. The variable on the horizontal axis is the eigenvalue of the network Laplacian displayed in a logarithmic scale, $\ln(-\Lambda)$. Blue dots indicate the growth rates for the original network, red dots are the ones after link deletion. The dashed curve is the dispersion relation for $\Delta\sigma = 0$. Positive values of $\Delta\sigma$ shift the dispersion relation upwards, yielding the dispersion relation used for evaluating pattern diversity (shown as a full line). Note that λ_s and λ_s^* are meant as distances from zero and hence are positive.

Figure 3 shows the region of the dispersion relation near zero growth rate with all unstable modes and adjacent stable modes. The relevant measures for prediction of topological sensitivity are: (i) the growth rate of the unstable modes for the original network, λ_u and after link deletion, λ_u^* and (ii) the weakest growth rate of the stable modes for the original network, λ_s and after link deletion, λ_s^*.

The relative size of these parameters and the number of unstable modes before (s) and after (s^*) dropping

a link suggests to classify the pattern into six different types of pattern sensitivity, color coded in Fig. 4 with the formal criteria listed as Boolean expressions. There are three criteria for high sensitivity of pattern diversity to topological perturbations: (1) the perturbation should destroy or establish (approximate) growth rate degeneracy of the unstable modes; (2) no weakly stable modes close to the instability threshold and (3) the growth rates of the (approximately degenerate) unstable modes should not be too small. The topological perturbations producing the strongest signals thus trigger a transition from two unstable modes with degenerate growth rates to a single unstable mode, while avoiding all interfering factors (stable modes close to the instability threshold, too small growth rates of unstable modes). In Fig. 3 the applicable classification for this specific dispersion relation is shown, predicting slightly less pattern diversity (color coded as light blue). Note that our prediction scheme summarized in Fig. 3 and applied, e.g., in Fig. 4 is a heuristic derived from studying the influencing factors of pattern diversity for a large set of numerical examples. The factor 1/2 in the requirement of a small enough distance of λ_u^* to the maximum of the dispersion relation has been chosen arbitrarily and a broader study of influencing factors might lead to a refined heuristic.

Figure 4 illustrates the relevance of the classification scheme for a full analysis of Turing pattern diversity changes under link removal for a random regular graph of degree 4, with 28 nodes and 60 links. Panels (A) and (B) show the change in pattern diversity for a specific pattern characterized by an unstable eigenvector, upon removal of a single link in a regular random graph. They are similar to the ones we showed in Figures 1 and 2 for the macaque cortical area network and for the ring graphs with one shortcut. While panels (A) and (B) show a specific case, panels (C) and (D) analyze the sensitivity of all possible patterns to the removal of any single link. Both, the GRDON and GRDPN parameter selection schemes are run for each eigenvector e_k separately. In this way we explore systematically the whole variety of situations displaying growth rate degeneracy.

Summarizing Fig. 4 we note that for this choice of the dispersion relation shift (via the additive constant $\Delta\sigma$ to the diffusion constant ratio σ, see Methods; see Supplementary Table S1) eigenvectors with low index are not influenced by the link removal. Low eigenvector indices correspond by definition to eigenvalues of small absolute size and we observe sensitivity to link removal in this regime only for higher values of $\Delta\sigma$. As discussed, strong changes in pattern diversity are triggered by a transition from two unstable modes with degenerate growth rates to a single unstable mode. We observe that for this parameter set and for random regular graphs, small eigenvalues of the graph Laplacian do not move much under link removal, making it unlikely that the associated patterns change stability. While we find this to be true for most of our parameter sets, we have not explored this in general for random regular graphs. However, note that this is also true (and intuitive) for the ring graphs: small eigenvalues correspond to long wavelength patterns. The distance between neighboring eigenvalues is much larger for long wavelengths than for short ones, making them more robust against perturbations.

We furthermore observe that the eigenvector determines whether the link removal leads to an increase, a decrease or no change in the pattern diversity. Specifically, eigenvectors that display growth rate degeneracy lead to changes of the pattern diversity.

DISCUSSION

Turing patterns in a continuum have been studied in great detail for many years, specifically their dependence on the parameters of the pattern-generating reaction diffusion system. Turing patterns on graphs offer a completely new way to influence the pattern formation by changing the underlying graph, e.g. adding or subtracting a small number of links. One important feature of Turing pattern formation on graphs evidenced in our study is the rarity of the emergence of a unique pattern. Even close to the instability threshold one often encounters a large number of simultaneously emerging stable patterns. They manifest themselves as a result of random sampling of initial conditions, a situation we call pattern diversity. Our study is a first step towards a full understanding of the mechanisms that generate such high diversity of patterns and its changes as the underlying graph undergoes small changes in its topology.

Our focus is on patterns determined by the unstable modes of the linear system, i.e. supercritical bifurcations. In particular, we do not consider the case of subcritical bifurcation where we are unable to relate pattern diversity to any topological features of the graph. In the supercritical case we can separate the influence of the reaction system from the influence of the underlying graph. The former is reflected in the dispersion relation determined by the parameters of the reaction system while the latter is a reflection of the eigenvalue spectrum of the graph Laplacian.

Our approach to disentangle the influence of the reaction parameters from the influence of the graph is based on the fact that the dispersion relation is locally quadratic (as in Fig. 3), and its width and location can only be changed by the reaction parameters. The part of the dispersion relation that lies above the zero growth rate determines the potential eigenvalues and associated eigenvectors that determine the emerging patterns. The number of eigenvalues and their spacing in this interval is a characteristic of the underlying graph. In that way the dispersion relation acts like a magnifying glass on the eigenvalue spectrum of the graph Laplacian.

Our analysis shows that the spacing of Laplacian eigenvalues and their movement on the dispersion curve under small topological changes of the graph translates into robustness or sensitivity of pattern diversity. In particu-

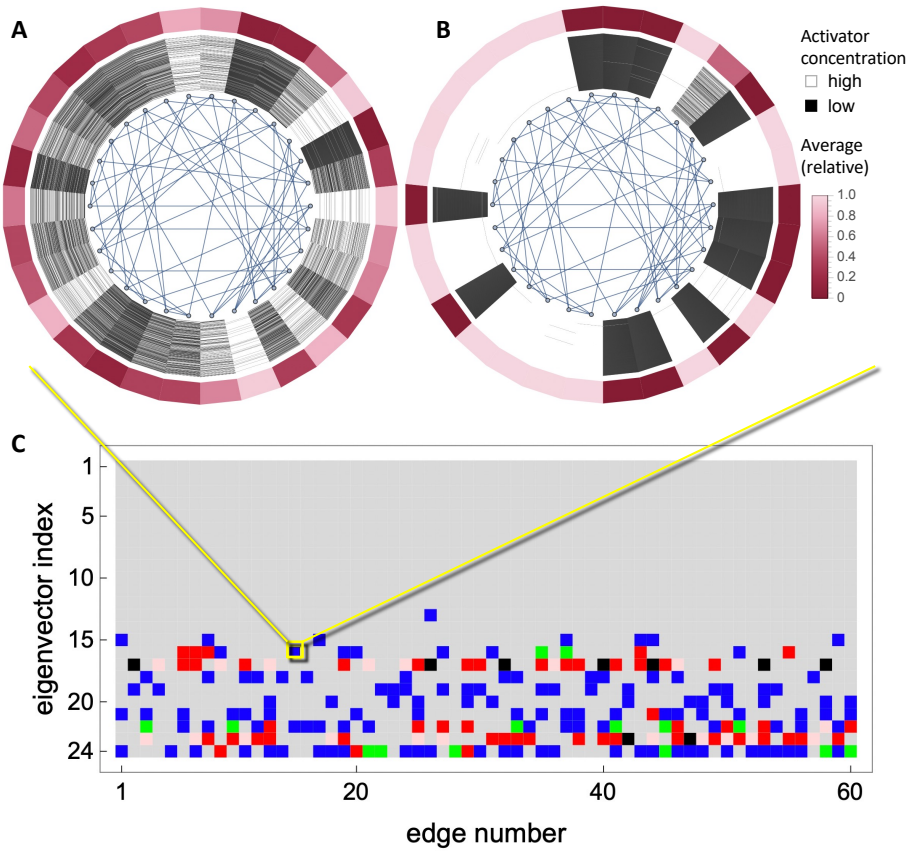

D

Color	Scheme	Criterion	Prediction
■	GRDON	$(\lvert s\rvert = 2) \wedge (\lvert s^*\rvert = 1) \wedge (\lambda_s > \lambda_u) \wedge (\lambda_u > \lambda_m/2) \wedge (\lambda_s^* > \lambda_u^*) \wedge (\lambda_u^* > \lambda_m/2)$	less pattern diversity
■	GRDON	$(\lvert s\rvert = 2) \wedge (\lvert s^*\rvert = 1) \wedge (\lambda_s > \lambda_u) \wedge (\lambda_s^* > \lambda_u^*)$	slightly less pattern diversity
■	GRDPN	$(\lvert s^*\rvert = 2) \wedge (\lvert s\rvert = 1) \wedge (\lambda_s > \lambda_u) \wedge (\lambda_u > \lambda_m/2) \wedge (\lambda_s^* > \lambda_u^*) \wedge (\lambda_u^* > \lambda_m/2)$	more pattern diversity
■	GRDPN	$(\lvert s^*\rvert = 2) \wedge (\lvert s\rvert = 1) \wedge (\lambda_s > \lambda_u) \wedge (\lambda_s^* > \lambda_u^*)$	slightly more pattern diversity
■	both	criteria for ■ and ■ fulfilled	dual change
■	GRDON	$(\lvert s\rvert > 2) \vee (\lvert s^*\rvert > 1)$	no change
■	GRDPN	$(\lvert s^*\rvert > 2) \vee (\lvert s\rvert > 1)$	no change
■	both	$(\lvert s\rvert = 0) \vee (\lvert s^*\rvert = 0)$	no patterns

FIG. 4. Predicting the impact of topological changes on pattern diversity. (A) Pattern wheel representation (see *Methods*) for 500 simulated patterns starting from random initial conditions under the GRD scheme of kinetic parameter selection (see *Methods*) for the original random regular graph and eigenvector 16. (B) Same as (A), but after removal of the link from node 4 to node 22. (C) Pattern diversity array (see *Methods*) depicting the *expected* change in Turing pattern diversity as a function of the deleted link index (horizontal axis) and the eigenvector label, eigenvectors being numbered at decreasing eigenvalues (vertical axis, recall that eigenvalues are negative). The parameter constellation investigated in (A) and (B) is highlighted in yellow. (D) Criteria defining the color code used in the pattern diversity array (C) and the corresponding prediction.

lar, small gaps between the unstable (or nearly unstable) eigenvalues surrounded by larger gaps can lead to high pattern diversity, whereas sequences of large gaps tend to favor a unique pattern.

These results are independent of the specific choice of the dynamical model or its parameters, as they only rely on the placement and the corresponding discrete sampling of the dispersion relation by the eigenvalues of the graph Laplacian. This discrete sampling is the determinant of pattern diversity.

One extreme case is the case of multiplicity of eigenvalues, e.g. due to symmetries, like in the case of a ring graph. Here the gap between two neighboring eigenvalues is zero leading to a continuum of patterns. Reaction parameters have no influence on this feature, but small changes of the underlying graph generically create a non-zero gap between the formerly degenerate eigenvalues and subsequently reduce the diversity of the emerging

patterns.

We extend the idea of small spectral gaps to the degeneracy of growth rates, i.e., situations where two adjacent eigenvalues of the graph Laplacian are not necessarily close in the spectrum but have the same growth rate. In order to systematically investigate these situations, we tune the reaction parameters such that the two adjacent eigenvalues are symmetrically distributed with respect to the maximum of the dispersion relation. A large number of numerical experiments for different types of graphs (small-world graphs [10], i.e., ring graphs with different numbers of shortcuts, ER graphs [45], random regular graphs and BA graphs [11]) show that pattern diversity changes significantly when small changes in the graph generate or destroy such approximate growth rate degeneracy.

CONCLUSION

Our study relates pattern forming capacities and spectral properties of networks. The variation in pattern diversity resulting from a change in network topology can be predicted by computing the change of the part of the eigenvalue spectrum of the graph Laplacian that is sampled by the unstable region of the dispersion curve. This link between the spectral properties of a graph and aspects pertaining to the robustness, predictability and controllability of self-organized patterns opens an avenue towards a better understanding of systemic vulnerabilities in network-like infrastructures relying on collective patterns.

ACKNOWLEDGMENTS

M. T. Hütt thanks LPTMC (Paris, Sorbonne Université and CNRS UMR 7600) for hospitality and the Physics Institute of CNRS (French National Center for Scientific Research) for funding his stays, during which part of this work has been performed. A. Lesne thanks Jacobs University, Bremen, for hospitality and CNRS for funding her stays.

AUTHOR CONTRIBUTIONS

All authors designed the study, carried out the analysis, and wrote the paper. D.A. performed the analytical computations presented in *Appendix A*. M.T.H performed numerical simulations.

COMPETING INTERESTS STATEMENT

The authors declare no competing financial interests.

Supplementary information accompanies this paper. Correspondence and requests for materials could be addressed to all authors.

Appendix A: Ring graph with shortcuts

We discuss two ways to generate topological sensitivity of pattern formation – one related to degenerate eigenvalues of the Laplacian created by symmetries, the other to degenerate growth rates, generated by two different but neighboring eigenvalues that are arranged in such a way that their growth rates are the same. To study the former, we consider a ring graph with a single shortcut as a minimal model. It offers the first step from spatially extended reaction-diffusion systems (here on a ring, as in the seminal work of Turing) to their counterpart on networks.

To simplify exposition we focus on a scalar reaction diffusion equation of the form

$$\frac{\partial u}{\partial t} = f(u) + Lu$$

where L is the Laplacian of the ring graph of N nodes and nearest-neighbor links given by

$$L_{i,j} = \begin{cases} 1 & \text{for } j = i-1 \\ 1 & \text{for } j = i+1 \\ -2 & \text{for } j = i \end{cases}$$

where i and j are integers modulo N. The eigenvalues of L are $\Lambda_q = -2(1 - \cos((k_q))$ where $k_q = 2\pi q/N$ for integer q. They are degenerate, each with multiplicity 2, and the associated eigenvectors are

$$\mathbf{X}_q(i) = \cos(k_q i), i = 0...N-1 \quad \text{and} \tag{A1}$$

$$\mathbf{Y}_q(i) = \sin(k_q i). \tag{A2}$$

Notice that any linear combination of these two eigenvectors (which is still an eigenvector with eigenvalue Λ_q) can be written in the amplitude-phase form $\tilde{\mathbf{u}}_k(i) = A\cos((k_q i) + \phi)$, corresponding to the fact that any embedding of the graph on a circle is invariant under the symmetry group of the circle. Following equivariant bifurcation theory [42] the generic steady state bifurcation can be described by a bifurcation on a 2-dimensional center manifold which leads to an invariant circle of fixed points. If the bifurcation is supercritical then the circle of fixed points is normally stable and has a zero eigenvalue in the tangential direction to the circle. Hence for uniformly randomly distributed initial conditions we expect uniform distributions of fixed points on the circle, representing patterns with a uniform distribution of phase shifts. We thus proved that the Gierer-Meinhardt model on the ring graph has a uniformly distributed ensemble of patterns around the circle. The average over patterns obtained with random initial conditions is therefore uniform, provided the number of patterns is large enough to avoid finite-sampling effects.

Laplacian eigenvalues for the ring graph with one shortcut

As discussed in the previous section, due to the symmetry of the ring graph, the eigenvalues Λ_q of its Laplacian have multiplicity two. The interlacing theorem [43, 44] applied to the addition of edges of a graph can be formulated in the following way:
Theorem: Let G be a graph with n vertices and let G^* be obtained from G by adding an edge joining distinct vertices of G and let $L(G^*), L(G)$ be the corresponding Laplacians. Then

$$\Lambda_{i-1}(L(G^*) \leq \Lambda_i(G) \leq \Lambda_i(G^*),$$

for all $i = 1, ..., n$. Thus, since the addition of an edge breaks the symmetry of the ring, the eigenvalues are non-degenerate and the eigenvalues of $L(G)$ interlace with the eigenvalues of $L(G^*)$. Since our variable on the horizontal axis for the dispersion curve is $\ln(-\Lambda)$, the eigenvalues of the ring graph with one shortcut move to the right on the dispersion curve, relative to the eigenvalues of the ring graph.

Suppl. Fig. S1 shows the spectrum and a typical eigenvector for the ring graph (panel A and C) and the ring graph with one shortcut (panel B and D), while Suppl. Fig. S2 and Suppl. Movie 1 show precisely how changing the shortcut position changes the number and eigenvalues of the unstable eigenvectors.

For the ring graph, the degenerate eigenvalues correspond to eigenvectors that are generated by even and odd sinusoidal functions with a free phase parameter. Thus for each shortcut, we can shift the phase parameter in such a way that one of the eigenvectors is even and the other is odd with respect to a reflection at the middle of the shortcut. Thus a theorem from graph theory called the edge principle [46, 47] can be used, which states that if $\mathbf{X}$ is eigenvector of the graph Laplacian with eigenvalue Λ satisfying $\mathbf{X}(i_0) = \mathbf{X}(i_s)$, then the Laplacian of a graph with the shortcut (i_0, i_s) has also $\mathbf{X}$ as an eigenvector with eigenvalue Λ. Thus for each pair of degenerate eigenvectors for the ring graph, the even eigenvector will be also an eigenvector with the same eigenvalue for the ring graph with a shortcut, i.e. a sinusoid with an appropriate phase shift as seen in Suppl. Fig. S1(D) (dashed line). As the eigenvector is the same, so is the eigenvalue. Hence, for each pair of degenerate eigenvalues of the Laplacian of the ring graph, one eigenvalue will be an eigenvalue for the ring graph with a shortcut and, following the interlacing theorem, the second one will move to the right but never cross the next eigenvalue of the ring graph.

Pattern diversity for the ring graph with one shortcut

We can recover these graph theoretic results and generate new insight by performing the analysis for eigenvectors of the Laplacian on the ring graph associated with the eigenvalue Λ_q and the wavelength $l = N/q$ and a shortcut from node i_0 to node i_s. The physical intuition for the edge principle discussed in the previous section is the following: A ring graph has sinusoidal eigenvectors. Any link that connects two nodes exactly one wavelength apart will have no impact on the eigenvectors. This can easily be seen when we write out the the expression for the eigenvalue of the Laplacian for the node i_0:

$$\sum_j L_{0j}u_j = u(i_{-1}) - u(i_0) + u(i_1) - u(i_0) + u(i_s) - u(i_0). \tag{A3}$$

When $u(i_0) = u(i_s)$ this expression becomes the same as in the ring graph, i.e. the shortcut has no influence. It is easy to see that the same is true for the time evolution of $u(i_s)$. Hence, for any eigenvector with a wavelength that approximately fits into the spacing of the ring graph, there exist shortcuts that have no influence and therefore any linear combination of the two eigenvectors of the ring graph will still be invariant under any phase shift leading to a uniformly distributed ensemble of patterns around the circle and thus to maximal pattern diversity.

A generic shortcut cuts the ring into pieces which, as evidenced by the geometry has a reflection symmetry relative to a reflection on a line that is perpendicular to the shortcut through its midpoint. By representation theory of the $Z(2)$ symmetry we will have an eigenfunction that is invariant under the reflection, i.e. even and another one that has a -1 representation, i.e. is an odd function. This is most easily illustrated for the eigenfunction with wavelength $l = N$, i.e. the cosine function $\cos(2\pi i/N)$: If the shortcut connects node i to node $N - i$ we have that

$$\cos\left(2\pi\frac{N-i}{N}\right) = \cos\left(2\pi(1 - \frac{1}{N}\right) = \cos\left(2\pi\frac{i}{N}\right),$$

i.e. the value of the activator is the same at the endpoints of the shortcut and thus the eigenfunction is even. Thus for every shortcut, there is a reflection-symmetric pattern that is selected by the shortcut as the even eigenfunction from the continuum of eigenfunctions in the amplitude-phase form of the ring graph. The associated eigenvalue is therefore the same as for the ring graph and, for N even (or N large), the amplitude of the node midway between the shortcut nodes is a maximum or minimum.

The corresponding second eigenfunction of the ring graph will be anti-symmetric and thus will have that $u(i_0) = -u(i_s)$. Inserting this into Eq. (A3) shows that this function is not an eigenfunction of the ring graph with a shortcut. Thus the eigenvalue for the antisymmetric eigenfunction of the ring graph with a shortcut will move and, for N even (or N large), the amplitude of the node midway between the shortcut nodes is zero (or approximately zero).

As we fix i_0 and move the endpoint i_s of the shortcut from one node to the next, we therefore observe a splitting of the degenerate eigenvalues of the ring graph

illustrated in Suppl. Fig. S1. Degenerate eigenvalues correspond to a continuum of patterns, while split eigenvalues show a small, finite number of patterns. This fully explains the diversity of the pattern formation in the ring graph with one shortcut. Suppl. Fig. S3 on the left panels shows the position of the eigenvalues on the dispersion relation as the shortcut moves and on the right panels shows the corresponding histograms of maximal correlations between the observed patterns in a set of 500 random initial conditions and the set of unstable eigenvectors. As the eigenvalues become degenerate (panel C and E), the growth rate for the associated eigenfunctions are very close. Hence, we expect that the final pattern is a linear combination of the two orthogonal eigenfunctions with about equal contributions. Measuring the correlation of that final pattern with one of the two eigenfunctions will lead to a projection of length $1/\sqrt{2}$, as one can see in panels D and F.

Numerical calculations of the anti-symmetric eigenvector shows, that the eigenvector corresponding to the moving eigenvalue evidently consists of two parts, each with the same wavelength but different amplitudes and phases. This suggests an Ansatz for an eigenfunction that is sinusoidal, with the same wavelength everywhere and where amplitude and phase of the two parts of the eigenfunctions have to be adjusted to satisfy continuity conditions and the eigenvalue is given by the relationship between the wavelength and the eigenvalue of the undisturbed ring graph

$$\Lambda = \Lambda_q = -2\left(1 - \cos(k_q)\right). \tag{A4}$$

Thus, the following calculation creates the eigenvalues as a function of the shortcuts like in Figure 2C. We assume without loss of generality that one end of the shortcut starts at node $n = 1$ and the shortcut ends at node y. The symmetry axis related to the Z(2) symmetry goes through the points $i^* = (1+y)/2$ and $j^* = (y+N+1)/2$ which are nodes of the ring, if i^* and j^* are integer and otherwise are just coordinates on the ring. Since we are looking for the odd eigenfunction, we have $u(1) = -u(y)$. In general for finite number of oscillators our assumption implies that the eigenfunctions are of the form $a\sin(k(i-i^*))$ on $i = 1...y$ and $\sin(k(i-j^*))$ on $i = y...N$. We have w.l.o.g. set the amplitude for the second part of the eigenfunction to one and leave the amplitude for the first part to be determined.

The eigenvalue of the network Laplacian for the nodes that are involved with the shortcut at node $i = 1$ and $i = y$ can be written as

$$u(0) - u(1) + u(2) - u(1) + u(y) - u(1) = \Lambda u(1),$$
$$u(y-1) - u(y) + u(y+1) - u(y) + u(1) - u(y) = \Lambda u(y),$$

which simplifies to

$$u(0) - 4u(1) + u(2) = \Lambda u(1). \tag{A5}$$

Assuming sinusoidal eigenfunctions we can evaluate them at these nodes to get:

$$u(1) = a\sin\left(k_q(1-i^*)\right) = -a\sin\left(k_q\left(\frac{y-1}{2}\right)\right)$$
$$u(2) = a\sin\left(k_q(2-i^*)\right) = -a\sin\left(k_q\left(\frac{y-3}{2}\right)\right)$$
$$u(y) = a\sin\left(k_q(y-i^*)\right) = a\sin\left(k_q\left(\frac{y-1}{2}\right)\right)$$
$$u(0) = u(N) = \sin\left(k(N-j^*)\right) = \sin\left(k_q\left(\frac{N-y-1}{2}\right)\right).$$

Inserting these into Equation (A5) gives

$$\sin\left(k_q\left(\frac{y+1-N}{2}\right)\right) + a\sin\left(k_q\left(\frac{y-3}{2}\right)\right) = (\Lambda+4)a\sin\left(k_q\left(\frac{y-1}{2}\right)\right) \tag{A6}$$

for the three unknowns a, k, Λ. Finally there is a continuity condition, which is that at node $i = 1$ and at node $i = y$ the two sinusoidal parts of the eigenvector have to have the same value. Hence

$$u(y) = -a\sin\left(k_q\left(\frac{y-1}{2}\right)\right) = \sin\left(k_q\left(\frac{N+1-y}{2}\right)\right). \tag{A7}$$

We can thus solve Equations (A4, A6 and A7) for a, k_q, Λ numerically. Note that these equations have $N/2$ solutions for k_q, corresponding to the number of eigenvalues for the even eigenmodes of the ring graph. To find a particular one, we have to restrict the numerical search

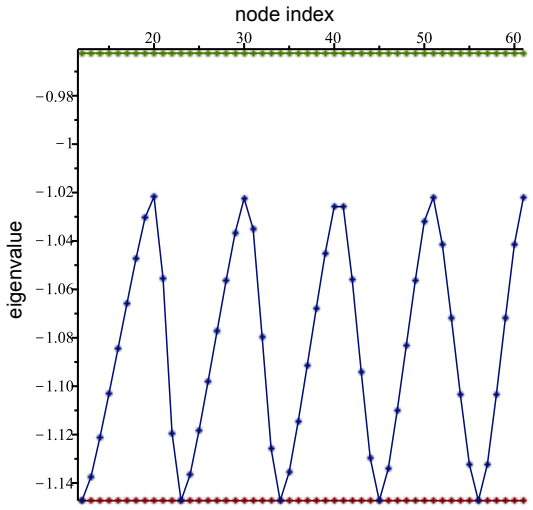

FIG. 5. Movement of the eigenvalue of the network Laplacian for a ring graph as a function of the endpoint of the shortcut. The starting point of the shortcut is always oscillator 1. The two eigenvalues at the top and bottom are the ones that do not depend on the shortcut.

to the interval between two eigenvalues of the ring graph without a shortcut. Figure 5 shows the movement of an eigenvalue of the network Laplacian as a function of the shortcut position.

We can also understand the primary bifurcations of this $2N$-dimensional dynamical system based on the symmetries of the eigenfunctions: when we add a shortcut, we break the D_n rotational symmetry of the ring graph. However for just one shortcut there is still a reflection symmetry at the midpoint of the shortcut. Thus we get an eigenfunction that is even with respect to that symmetry and one that is odd, corresponding to the two cases discussed above. The eigenfunction that is odd corresponds to a (-1)-representation of the $Z(2)$ symmetry leading to pitchfork bifurcations [42]. The $Z(2)$ symmetry places no restrictions on the bifurcations for the even eigenfunction. However, since this eigenfunction inherits the sinusoidal structure of the ring graph, it generates a (-1)-representation under a translation along the ring graph by half a wavelength. Hence the primary bifurcation for both modes will be pitchfork bifurcations and thus no subcritical modes will appear in a ring graph with just one shortcut. This will change as the number of shortcuts increases [48].

Pattern diversity analysis for the ring graph with two shortcuts

We observed the same set of phenomena when we add a second shortcut and move its end while the first shortcut is kept fixed. Supplementary Figure S5 displays the predictability scheme (analog of Fig. 4) for the ring graph with two shortcuts. Note that case A is again close to a degeneracy and therefore exhibits high pattern diversity.

[1] A. M. Turing, The chemical basis of morphogenesis, Phil. Trans. Roy. Soc. of London, Series B **237**, 37 (1952).

[2] A. Gierer and H. Meinhardt, A theory of biological pattern formation, Kybernetik **12**, 30 (1972).

[3] J. B. Green and J. Sharpe, Positional information and reaction-diffusion: two big ideas in developmental biology combine, Development **142**, 1203 (2015).

[4] I. Prigogine, Dissipative structures in chemical systems, in *Fast reactions and primary processes in chemical kinetics: Proceedings of the fifth Nobel symposium held August 28-September 2, 1967* (1967) pp. 371–382.

[5] D. Walgraef, *Spatio-temporal pattern formation: with examples from physics, chemistry, and materials science* (Springer Science & Business Media, 2012).

[6] A. Goldbeter, Dissipative structures in biological systems: bistability, oscillations, spatial patterns and waves, Philosophical Transactions of the Royal Society A: Mathematical, Physical and Engineering Sciences **376**, 20170376 (2018).

[7] R. A. Satnoianu, M. Menzinger, and P. K. Maini, Turing instabilities in general systems, Journal of Mathematical Biology **41**, 493 (2000).

[8] H. Nakao and A. S. Mikhailov, Turing patterns in network-organized activator-inhibitor systems, Nature Physics **6**, 544 (2010).

[9] R. Pastor-Satorras and A. Vespignani, Patterns of complexity, Nature Physics **6**, 480 (2010).

[10] D. J. Watts and S. H. Strogatz, Collective dynamics of 'small-world' networks, Nature **393**, 440 (1998).

[11] A.-L. Barabási and R. Albert, Emergence of scaling in random networks, Science **286**, 509 (1999).

[12] R. Albert and A.-L. Barabási, Statistical mechanics of complex networks, Reviews of Modern Physics **74**, 47 (2002).

[13] S. H. Strogatz, Exploring complex networks, Nature **410**, 268 (2001).

[14] M. E. Newman, The structure and function of complex networks, SIAM Review **45**, 167 (2003).

[15] S. Boccaletti, V. Latora, Y. Moreno, M. Chavez, and D.-U. Hwang, Complex networks: Structure and dynamics, Physics Reports **424**, 175 (2006).

[16] F. A. Rodrigues, T. K. D. Peron, P. Ji, and J. Kurths, The Kuramoto model in complex networks, Physics Reports **610**, 1 (2016).

[17] A. Arenas, A. Díaz-Guilera, J. Kurths, Y. Moreno, and C. Zhou, Synchronization in complex networks, Physics Reports **469**, 93 (2008).

[18] X. Zhang, S. Hallerberg, M. Matthiae, D. Witthaut, and M. Timme, Fluctuation-induced distributed resonances in oscillatory networks, Science Advances **5**, eaav1027 (2019).

[19] S. N. Dorogovtsev, A. V. Goltsev, and J. F. Mendes, Critical phenomena in complex networks, Reviews of Modern Physics **80**, 1275 (2008).

[20] P. Nyczka, M.-T. Hütt, and A. Lesne, Inferring pattern generators on networks, Physica A: Statistical Mechanics and its Applications **566**, 125631 (2021).

[21] M. Müller-Linow, C. C. Hilgetag, and M.-T. Hütt, Organization of excitable dynamics in hierarchical biological networks., PLoS Computational Biology **4**, e1000190 (2008).

[22] P. Moretti and M.-T. Hütt, Link-usage asymmetry and collective patterns emerging from rich-club organization of complex networks, PNAS **117**, 18332 (2020).

[23] A. Lesne, Complex networks: from graph theory to biology, Letters in Mathematical Physics **78**, 235 (2006).

[24] M. Hütt and A. Lesne, Interplay between topology and dynamics in excitation patterns on hierarchical graphs, Frontiers in neuroinformatics **3**, 28 (2009).

[25] D. Armbruster, C. de Beer, M. Freitag, T. Jagalski, and C. Ringhofer, Autonomous control of production networks using a pheromone approach, Physica A: Statistical Mechanics and its applications **363**, 104 (2006).

[26] A. Vespignani, The fragility of interdependency, Nature **464**, 984 (2010).

[27] W.-X. Wang, Y.-C. Lai, and D. Armbruster, Cascading failures and the emergence of cooperation in evolutionary-game based models of social and economical networks, Chaos: An Interdisciplinary Journal of Nonlinear Science **21**, 033112 (2011).

[28] R. Pastor-Satorras, C. Castellano, P. Van Mieghem, and A. Vespignani, Epidemic processes in complex networks, Reviews of Modern Physics **87**, 925 (2015).

[29] H. Blunck, D. Armbruster, J. Bendul, and M.-T. Hütt, The balance of autonomous and centralized control in scheduling problems, Applied Network Science **3**, 1 (2018).

[30] D. Mateo, N. Horsevad, V. Hassani, M. Chamanbaz, and R. Bouffanais, Optimal network topology for responsive collective behavior, Science Advances **5**, eaau0999 (2019).

[31] R. J. Gallagher, J.-G. Young, and B. F. Welles, A clarified typology of core-periphery structure in networks, Science Advances **7**, eabc9800 (2021).

[32] R. Muolo, M. Asllani, D. Fanelli, P. K. Maini, and T. Carletti, Patterns of non-normality in networked systems, Journal of theoretical biology **480**, 81 (2019).

[33] S. Mimar, M. M. Juane, J. Park, A. P. Munuzuri, and G. Ghoshal, Turing patterns mediated by network topology in homogeneous active systems, Physical Review E **99**, 062303 (2019).

[34] T. Carletti and H. Nakao, Turing patterns in a network-reduced FitzHugh-Nagumo model, Physical Review E **101**, 022203 (2020).

[35] C. Liu, L. Chang, Y. Huang, and Z. Wang, Turing patterns in a predator–prey model on complex networks, Nonlinear Dynamics , 1 (2020).

[36] P. S. Putra, H. Susanto, and N. Nuraini, Turing patterns of non-linear SI model on random and real-structure networks with diarrhea data, Scientific reports **9**, 1 (2019).

[37] N. T. Markov, M. Ercsey-Ravasz, A. Ribeiro Gomes, C. Lamy, L. Magrou, J. Vezoli, P. Misery, A. Falchier, R. Quilodran, M. Gariel, *et al.*, A weighted and directed interareal connectivity matrix for macaque cerebral cortex, Cerebral cortex **24**, 17 (2014).

[38] R. Morecraft, K. Stilwell-Morecraft, P. Cipolloni, J. Ge, D. McNeal, and D. Pandya, Cytoarchitecture and cortical connections of the anterior cingulate and adjacent somatomotor fields in the rhesus monkey, Brain research bulletin **87**, 457 (2012).

[39] R. Morecraft, K. Stilwell-Morecraft, J. Ge, P. Cipolloni, and D. Pandya, Cytoarchitecture and cortical connections of the anterior insula and adjacent frontal motor fields in the rhesus monkey, Brain research bulletin **119**, 52 (2015).

[40] M. E. Newman, *Networks* (Oxford University Press, 2018).

[41] M.-T. Hütt, M. Kaiser, and C. C. Hilgetag, Perspective: network-guided pattern formation of neural dynamics, Philosophical Transactions of the Royal Society B: Biological Sciences **369**, 20130522 (2014).

[42] M. Golubitsky, I. Stewart, and D. G. Schaeffer, *Singularities and Groups in Bifurcation Theory: Volume II*, Vol. 69 (Springer Science & Business Media, 2012).

[43] B. Mohar, The Laplacian spectrum of graphs, Graph theory, combinatorics, and applications **2**, 12 (1991).

[44] A. E. Brouwer and W. H. Haemers, *Spectra of graphs* (Springer Science & Business Media, 2011).

[45] P. Erdős and A. Rényi, On the evolution of random graphs, Publ. Math. Inst. Hung. Acad. Sci **5**, 17 (1960).

[46] R. Merris, Laplacian graph eigenvectors, Linear algebra and its applications **278**, 221 (1998).

[47] M. W. Newman, The Laplacian spectrum of graphs, (2001), master Thesis dissertation, University of Manitoba, Canada.

[48] M. Wolfrum, The Turing bifurcation in network systems: Collective patterns and single differentiated nodes, Physica D: Nonlinear Phenomena **241**, 1351 (2012).